The Astrophysical Journal, 624:571–585, 2005 May 10

SPECTROSCOPIC PROPERTIES OF VOID GALAXIES IN THE SLOAN DIGITAL SKY SURVEY

Randall R. Rojas,[1] Michael S. Vogeley,[1] Fiona Hoyle,[1] and Jon Brinkmann[2]

Received 2004 September 3; accepted 2004 December 22

ABSTRACT

We study the spectroscopic properties of a sample of 10^3 void galaxies identified in the Sloan Digital Sky Survey (SDSS) and compare these with the properties of galaxies in higher density regions (wall galaxies). This sample of void galaxies covers the range of absolute magnitude from $M_r = -13.5$ to $M_r = -22.5$ in regions with density contrast $\delta\rho/\rho < -0.6$. We compare the equivalent widths of Hα, [O II], [N II], Hβ, and [O III] of void and wall galaxies with similar luminosities. We find that void galaxies have larger emission line equivalent widths, indicating that they are forming stars at a higher rate. A comparison of the Balmer break, as measured by the parameter $D_n(4000)$, reveals that void galaxies have younger stellar populations than wall galaxies. Using standard techniques, we estimate Hα and [O II] star formation rates (SFRs) of the void and wall galaxies. Combining these measurements with estimates of the stellar masses, we find specific star formation rates (SFR per unit stellar mass) for void galaxies that are generally higher than for wall galaxies, consistent with the results from the equivalent widths.

Subject headings: cosmology: observations — galaxies: stellar content — large-scale structure of universe — methods: statistical

Online material: color figures

1. INTRODUCTION

Studying the variation of galaxy properties within environment is fundamental to our understanding of galaxy formation and evolution. Dressler (1980) characterized the morphology-density relation as the tendency for elliptical galaxies to reside in clusters and spirals in the field. This trend has been confirmed by many different groups (e.g., Postman & Geller 1984; Zabludoff & Mulchaey 1998; Hashimoto & Oemler 1999; Tran et al. 2001; Dominguez et al 2001; Treu et al. 2003). Recent studies have attempted to extend the study of this environmental dependence into increasingly underdense regions. In a series of papers (Rojas et al. 2004; Hoyle et al. 2005; Goldberg et al. 2005), we seek to examine if galaxies that reside in the most underdense regions, referred to as void galaxies, are fundamentally different from galaxies in denser environments.

Many studies have also shown that there is a strong dependence of star formation on environment. High star formation rates (SFRs) are usually found in relatively low density environments, while lower SFRs are more commonly seen in higher density regions (Dressler et al. 1985; Couch & Sharples 1987; Balogh et al. 1997, 1998, 1999, 2002; Hashimoto et al. 1998; Poggianti et al. 1999; Couch et al. 2001; Solanes et al. 2001; Lewis at al. 2002; Gomez et al. 2003). However, only recently was it possible to show that there is a strong dependence of SFR on local galaxy density, using samples that were large enough to include a fair mix of morphological types. Gomez et al. (2003) showed that there is a decrease in SFR from galaxies in the field to galaxies in denser environments (e.g., in rich clusters). Independently, Lewis et al. (2002) found the same strong correlation between environment and SFRs in the Two-Degree Field (2dF) Galaxy Redshift Survey. Hashimoto et al. (1998) noted that, regardless of the concentration index, galaxies in clusters have on average lower SFRs than field galaxies in the Las Campanas Redshift Survey. As a measure of SFR, some groups consider the strength of Hα emission and consistently find that Hα emission has a strong dependence on local density (Balogh et al. 2004; Tanaka et al. 2004). Efforts to extrapolate the density-SFR relation to lower densities have met with some success. However, none have been able to probe the very lowest densities.

Void galaxies have been studied photometrically by Grogin & Geller (1999) and by Rojas et al. (2004). They demonstrated that there are significant differences between void and nonvoid galaxies, with void galaxies being bluer in color and having morphologies that more closely resembled late-type galaxies. However, they found that this was not simply an extension of the morphology-density relation; late-type galaxies in low-density environments were bluer than late-type galaxies in higher density environments. This suggests that environment not only influences the relative morphological mix of galaxies but also helps determine the properties of galaxies of fixed morphology.

In this paper, we focus on the spectroscopic properties of void galaxies, to examine the role of density on the strength of the equivalent widths (EWs) of various lines and on SFRs. Related work includes the analysis by Grogin & Geller (2000), who analyzed a sample of 150 low-density galaxies with $\delta\rho/\rho < 0.0$, including 46 galaxies at density contrast $\delta\rho/\rho < -0.5$. Grogin & Geller showed that the EW(Hα)-density relation is most noticeable in either the lowest or highest density environments, i.e., the void galaxies had large EW(Hα), and the galaxies in richer environments had smaller values of EW(Hα). We extend this work by using a sample of 10^3 void galaxies with density contrast $\delta\rho/\rho < -0.6$ that spans a broad range of absolute magnitude from $M_r = -13.5$ to $M_r = -22.5$. We use this sample to quantitatively extend the study of star formation history down to the lowest densities possible and compare the spectroscopic properties of our void galaxies with nonvoid galaxies of similar luminosities and surface brightness profiles. These comparisons are crucial in order to constrain models of galaxy formation and evolution.

[1] Department of Physics, Drexel University, 3141 Chestnut Street, Philadelphia, PA 19104; rrojas@mercury.physics.drexel.edu, vogeley@drexel.edu, fiona.hoyle@drexel.edu.

[2] Apache Point Observatory, P.O. Box 59, Sunspot, NM 88349-0059.

In § 2 we discuss the data sample. In §§ 3 and 4 we present the results of the various spectroscopic parameters. We compare the results with those from other groups in § 5. Finally, in § 6 we present our conclusions.

2. THE DATA

We identify a sample of 10^3 void galaxies from early data available from the Sloan Digital Sky Survey (SDSS). The SDSS is a wide-field photometric and spectroscopic survey that will cover approximately 10^4 deg^2. CCD imaging of 10^8 galaxies in five colors and follow-up spectroscopy of 10^6 galaxies with $r < 17.77$ will be obtained. York et al. (2000) provide an overview of the SDSS, and Stoughton et al. (2002) describe the early data release (EDR) and details about the photometric and spectroscopic measurements, and Abazajian et al. (2003, 2004) describe the first (DR1) and second (DR2) data releases. Technical articles providing details of the SDSS include descriptions of the photometric camera (Gunn et al. 1998), photometric analysis (Lupton et al. 2005, in preparation), the photometric system (Fukugita et al. 1996; Smith et al. 2002), the photometric monitor (Hogg et al. 2001), astrometric calibration (Pier et al. 2003), the selection of the galaxy spectroscopic samples (Strauss et al. 2002; Eisenstein et al. 2001), and spectroscopic tiling (Blanton et al. 2003a). A thorough analysis of possible systematic uncertainties in the galaxy samples is described in Scranton et al. (2002). All the galaxies are *k*-corrected according to Blanton et al. (2003c), and we assume a $\Omega_m = 0.3$, $\Omega_\Lambda = 0.7$ cosmology and Hubbles constant $h = H_0/100$ km s^{-1} Mpc^{-1} throughout.

In this paper, we consider the spectral properties of galaxies in different environments. The SDSS spectra cover the wavelength range 3900–9100 Å, obtained using a double blue/red spectrograph with the beam split at 6150 Å by a dichroic. The data have spectral resolution ranging from 1800 to 2100 (i.e., $\lambda/\delta\lambda \approx 2000$), so at 4000 Å the resolution is ~2 Å. The signal-to-noise ratio, S/N, is typically 13 per pixel.

Void galaxies are drawn from a sample referred to as "sample10" (Blanton et al. 2003b). This sample covers nearly 2000 deg^2 and contains 155,126 galaxies. We use a nearest-neighbor analysis, described in more detail below, to find galaxies that reside in regions of density contrast $\delta\rho/\rho < -0.6$, as measured on a scale of 7 h^{-1} Mpc. These are labeled as void galaxies. Galaxies with larger vales of $\delta\rho/\rho$ are referred to as wall galaxies. This choice of physical scale and density contrast yields samples of void galaxies that are consistent with samples obtained using other definitions of void regions, e.g., El-Ad & Piran (1997) and Hoyle & Vogeley (2002, 2004). In the latter work, we find that, in voids that are at least 10 h^{-1} Mpc in radius and that are underdense with $\delta\rho/\rho < -0.9$, the few galaxies in those voids have density contrast $\delta\rho/\rho < -0.6$ as measured on a scale of 7 h^{-1} Mpc (the density immediately around a void galaxy is higher than the average for the whole void, because galaxies are clustered).

Full details of void galaxy selection are described in Rojas et al. (2004). Here we provide a brief overview, as follows. First, a volume-limited sample of relatively bright galaxies is constructed to define the density field that traces the distribution of voids. This volume-limited sample extends to a maximum redshift of $z_{\max} = 0.089$. We identify void galaxies from the flux-limited sample, also truncated at $z = 0.089$. We discard galaxies that lie close to the edge of the survey, because it is impossible to tell whether a galaxy is a void galaxy if its neighbors have not yet been observed. For each of the remaining galaxies in the flux-limited sample, we measure the distance to its third nearest neighbor in the volume-limited catalog. A galaxy with fewer than three neighbors within a sphere of radius 7 h^{-1} Mpc is flagged as a void galaxy. Galaxies with more than three neighbors we label as wall galaxies. This procedure yields a sample of 1010 void galaxies and 12,732 wall galaxies. These void and wall galaxies span a redshift range $0.034 < z < 0.089$ and a range of absolute magnitudes from $-22 < M_r < -17.77$. This sample is referred to as the "distant" sample. We split this sample in half at an absolute magnitude of $M_r = -19.5$ to yield bright (WGD_b, VGD_b; $M_r \leq -19.5$; b = bright, W = wall, V = void) and faint (WGD_f, VGD_f; $M_r > -19.5$; f = faint) subsamples.

We also construct a sample of fainter and closer void galaxies, the "nearby" sample, by using the wider angle Updated Zwicky Catalog (UZC; Falco et al. 1999) and the Southern Sky Redshift Survey (SSRS; da Costa et al. 1998) to trace the distribution of local voids (see Fig. 1 in Rojas et al. 2004). We employ these other surveys because the slices of SDSS scans (which extend over roughly 2.°5 in declination) are too narrow in sample10 to accurately map the large-scale structure at small cosmological distance. We construct volume-limited samples of the UZC and SSRS2 to match the density of objects used as tracers for the distant sample of SDSS galaxies. The nearby sample extends to a maximum redshift of $z_{\max} = 0.025$. We apply the same nearest-neighbor analysis to identify an additional 194 void galaxies and 2256 wall galaxies from a flux-limited sample of nearby SDSS galaxies. The absolute magnitudes of these galaxies lie in the range $-19.7 < M_r < -13$. We split this nearby sample into bright (WGN_b, VGN_b; $M_r \leq -17$; b = bright) and faint (WGN_f, VGN_f; $M_r > -17$; f = faint) subsamples of approximately equal number. Note that the division into bright and faint subsamples occurs at different absolute magnitudes in the nearby and distant samples. This difference is necessary, because there are very few galaxies in the overlap in absolute magnitude between the nearby and bright samples.

3. MEASURED SPECTROSCOPIC PROPERTIES

In this paper we study the spectroscopic differences between void and wall galaxies. We compare their Hα, [O II] λ3727, Hβ, [N II] λ6583, [O III] λ5007 EWs and 4000 Å Balmer breaks (ratio of the average flux density in the bands 4050–4250 and 3750–3950 Å, $D_n(4000)$; Bruzual 1983).

We choose these quantities to examine a broad range of features in the spectra of our galaxies and star formation on different time scales. For example, the Hα line probes star formation on timescales of $\sim 10^7$ yr (lifetime of an H II region), whereas the 4000 Å break probes timescales of $t \sim 1$ Gyr.

These emission lines are sensitive to a range of properties of star formation regions. EW(Hα) measures the ratio of flux from recent star formation (mainly flux from UV photons, i.e., $\lambda < 912$ Å) to the integrated past star formation (predominantly flux from old stellar populations), whereas the [O II] forbidden line is due to UV radiation ($\lambda < 730$ Å) produced by massive stars that ionize heavier elements. The [O II] line's dependence on excitation and oxygen abundance makes it a somewhat less reliable measure of current star formation (Koo & Kron 1992). Note that [O II] cannot be detected in 90% of the nearby galaxies because it can only be measured by the SDSS at a redshift of $z \gtrsim 0.07$. Hence, no [O II] results are given for the nearby sample.

The strength of EW(Hα) is typically double that of [O II]. In both cases, large values of EW suggest high star formation. Large Hα EWs are directly related to high SFRs, bluer colors, and fainter absolute magnitudes (Kennicutt & Kent 1983). Strong correlations between EW([O II]) and galaxy colors have been shown to exist for various galaxy types and redshifts

TABLE 1
DISTANT SAMPLE

Property	Void ($\mu \pm \sigma_\mu$)	Wall ($\mu \pm \sigma_\mu$)	KS Probability (P)[a]	N_V, N_W
Full: $-22.5 \leq M_r \leq -17.77$, $N_V = 1010$, $N_W = 12732$				
EW(Hα) (Å)	19.14 ± 0.680	11.77 ± 0.158	$<10^{-4}$	1005, 12,636
EW([O II]) (Å)	14.26 ± 0.395	9.441 ± 0.093	$<10^{-4}$	1006, 12,301
EW(Hβ) (Å)	2.571 ± 0.146	0.828 ± 0.035	$<10^{-4}$	997, 12,544
EW([N II]) (Å)	6.553 ± 0.181	5.065 ± 0.049	$<10^{-4}$	1006, 12,586
EW([O III]) (Å)	4.694 ± 0.335	2.197 ± 0.061	$<10^{-4}$	994, 12,373
$D_n(4000)$	1.515 ± 0.011	1.649 ± 0.003	$<10^{-4}$	714, 9862
$\log_{10}(\text{mass}/M_\odot)$	10.13 ± 0.015	10.43 ± 0.004	$<10^{-4}$	1010, 12,732
SFR(Hα) ($M_\odot$ yr^{-1})	0.734 ± 0.025	0.747 ± 0.007	$<10^{-4}$	850, 8930
SFR([O II]) ($M_\odot$ yr^{-1})	0.448 ± 0.015	0.488 ± 0.006	$<10^{-4}$	841, 8764
S-SFR(Hα) (yr^{-1})	$(3.744 \pm 0.108) \times 10^{-11}$	$(2.629 \pm 0.034) \times 10^{-11}$	$<10^{-4}$	850, 8930
S-SFR([O II]) (yr^{-1})	$(4.892 \pm 0.890) \times 10^{-11}$	$(3.020 \pm 0.251) \times 10^{-11}$	$<10^{-4}$	841, 8764
Bright: $M_r \leq -19.5$, $N_V = 409$, $N_W = 7831$				
EW(Hα) (Å)	14.47 ± 0.932	8.542 ± 0.175	$<10^{-4}$	406, 7774
EW([O II]) (Å)	9.338 ± 0.429	6.884 ± 0.089	$<10^{-4}$	399, 7548
EW(Hβ) (Å)	1.246 ± 0.201	0.018 ± 0.038	$<10^{-4}$	401, 7699
EW([N II]) (Å)	6.606 ± 0.332	4.711 ± 0.066	$<10^{-4}$	407, 7743
EW([O III]) (Å)	2.706 ± 0.531	1.172 ± 0.055	$<10^{-4}$	401, 7574
$D_n(4000)$	1.602 ± 0.017	1.711 ± 0.004	$<10^{-4}$	287, 6069
$\log_{10}(\text{mass}/M_\odot)$	10.52 ± 0.016	10.70 ± 0.004	$<10^{-4}$	409, 7831
SFR(Hα) ($M_\odot$ yr^{-1})	1.136 ± 0.063	0.920 ± 0.016	$<10^{-4}$	306, 4956
SFR([O II]) ($M_\odot$ yr^{-1})	0.736 ± 0.051	0.626 ± 0.013	$<10^{-4}$	304, 4876
S-SFR(Hα) (yr^{-1})	$(3.133 \pm 0.169) \times 10^{-11}$	$(2.137 \pm 0.004) \times 10^{-11}$	$<10^{-4}$	306, 4956
S-SFR([O II]) (yr^{-1})	$(3.061 \pm 0.279) \times 10^{-11}$	$(2.192 \pm 0.053) \times 10^{-11}$	$<10^{-4}$	304, 4876
Faint: $M_r > -19.5$, $N_V = 601$, $N_W = 4901$				
EW(Hα) (Å)	22.31 ± 0.929	16.93 ± 0.287	$<10^{-4}$	599, 4862
EW([O II]) (Å)	17.57 ± 0.554	13.50 ± 0.178	$<10^{-4}$	593, 4753
EW(Hβ) (Å)	3.452 ± 0.202	2.095 ± 0.067	$<10^{-4}$	531, 4334
EW([N II]) (Å)	6.517 ± 0.204	5.630 ± 0.074	$<10^{-4}$	599, 4843
EW([O III]) (Å)	6.038 ± 0.423	3.817 ± 0.128	$<10^{-4}$	593, 4799
$D_n(4000)$	1.456 ± 0.013	1.551 ± 0.004	$<10^{-4}$	427, 3793
$\log_{10}(\text{mass}/M_\odot)$	9.873 ± 0.015	10.02 ± 0.005	$<10^{-4}$	601, 4901
SFR(Hα) ($M_\odot$ yr^{-1})	0.508 ± 0.0237	0.530 ± 0.009	0.0254	544, 3974
SFR([O II]) ($M_\odot$ yr^{-1})	0.286 ± 0.017	0.316 ± 0.007	0.0298	537, 3888
S-SFR(Hα) (yr^{-1})	$(4.146 \pm 0.137) \times 10^{-11}$	$(3.349 \pm 0.005) \times 10^{-11}$	$<10^{-4}$	544, 3974
S-SFR([O II]) (yr^{-1})	$(5.725 \pm 1.375) \times 10^{-11}$	$(4.058 \pm 0.147) \times 10^{-11}$	0.0034	537, 3888

NOTE.—Means, errors on the means, and KS test probabilities that the void and wall galaxies are drawn from the same parent population for the spectroscopic properties of void and wall galaxies in the distant sample ($100 \leq r \leq 260\,h^{-1}$ Mpc). The number of galaxies (void and wall) in each sample and subsample are listed next to the magnitude range heading as [N_V(void), N_W(wall)]. The KS test shows that the void and wall galaxies are drawn from different populations based on emission line EWs, stellar masses, Hα, and [O II] derived SFRs and S-SFRs, and $D_n(4000)$. The differences between the means of the different parameters measured are on average >5 σ_μ, except for the SFR(Hα) and SFR([O II]) in the faint subsample, where the difference is $\sim$2 σ_μ. Void galaxies on average have higher S-SFRs, larger EWs, smaller stellar masses, and smaller $D_n(4000)$.

[a] Small values of P correspond to a low probability that the two samples are drawn from the same parent population.

(Huchra 1977; Peterson et al. 1986; Broadhurst et al. 1988, 1992; Colless et al. 1990; Koo & Kron 1992).

We use the widths of the Gaussian fit to the respective lines as measured by the SDSS spectral pipeline ("spectro1d"; SubbaRao et al. 2002). For the 4000 Å break strength, we use Kauffmann et al's. (2003, hereafter K03) estimates of this index [$D_n(4000)$]. K03 produced these measurements for the SDSS DR1, which is somewhat smaller than the sample analyzed in this paper; thus, we restrict our analysis of $D_n(4000)$ to the 70% of our sample for which this quantity was measured. K03 measure $D_n(4000)$ using the ratio of the average flux density in narrow continuum bands (3850–3950 and 4000–4100 Å) as suggested by Balogh et al. (1999). The value of $D_n(4000)$ is an excellent indicator of past star formation on timescales of $t \sim 1$ Gyr and is also insensitive to dust attenuation. For hot stars where elements are multiply ionized, the opacity decreases. Therefore, hot, young stars (e.g., O and B) have lower amplitudes of $D_n(4000)$ than cooler, older stars (e.g., K and M; see Fig. 3, Bruzual 1983). Since late-type galaxies are mainly composed of young stars, their 4000 Å break is smaller than for early-type galaxies, which are primarily composed of older stellar populations.

We compute the means and the errors on the mean of the distributions of EWs and $D_n(4000)$s of void and wall galaxies. We also use the Kolmogorov-Smirnov (KS) test to examine whether the void and wall galaxies could be drawn from the same parent population based on the spectroscopic properties under consideration.

TABLE 2
NEARBY SAMPLE

Property	Void ($\mu \pm \sigma_\mu$)	Wall ($\mu \pm \sigma_\mu$)	KS Probability (P)[a]	N_V, N_W
Full: $-19.9 \leq M_r \leq -14.5$, $N_V = 194$, $N_W = 2256$				
EW(Hα) (Å)	35.31 ± 0.262	26.18 ± 0.645	0.0021	187, 2202
EW(Hβ) (Å)	7.317 ± 0.738	5.702 ± 0.242	0.0007	192, 2226
EW([N II]) (Å)	5.175 ± 0.338	4.298 ± 0.097	0.0611	191, 2232
EW([O III]) (Å)	18.50 ± 2.111	14.17 ± 0.548	$<10^{-4}$	188, 2211
$D_n(4000)$	1.261 ± 0.019	1.314 ± 0.005	$<10^{-4}$	119, 1545
$\log_{10}(\text{mass}/M_\odot)$	8.692 ± 0.060	8.803 ± 0.018	0.0592	194, 2256
SFR(Hα) ($M_\odot$ yr^{-1})	0.162 ± 0.012	0.146 ± 0.006	0.3410	183, 2020
S-SFR(Hα) (yr^{-1})	$(25.55 \pm 0.353) \times 10^{-11}$	$(31.70 \pm 0.169) \times 10^{-11}$	0.0001	182, 2005
Bright: $M_r \leq -17.0$, $N_V = 76$, $N_W = 1071$				
EW(Hα) (Å)	33.316 ± 3.74	21.91 ± 0.809	0.0005	76, 1060
EW(Hβ) (Å)	5.939 ± 0.769	3.770 ± 0.210	0.0006	76, 1055
EW([N II]) (Å)	7.223 ± 0.733	5.203 ± 0.157	0.0034	76, 1062
EW([O III]) (Å)	11.615 ± 2.41	8.276 ± 0.525	0.0133	76, 1056
$D_n(4000)$	1.287 ± 0.032	1.371 ± 0.008	$<10^{-4}$	50, 792
$\log_{10}(\text{mass}/M_\odot)$	9.333 ± 0.066	9.390 ± 0.018	0.4123	76, 1071
SFR(Hα) ($M_\odot$ yr^{-1})	0.323 ± 0.048	0.194 ± 0.011	0.0009	73, 933
S-SFR(Hα) (yr^{-1})	$(17.57 \pm 3.222) \times 10^{-11}$	$(12.57 \pm 0.958) \times 10^{-11}$	$<10^{-4}$	73, 933
Faint: $M_r > -17.0$, $N_V = 118$, $N_W = 1185$				
EW(Hα) (Å)	36.68 ± 3.60	30.14 ± 0.977	0.3740	111, 1142
EW(Hβ) (Å)	8.220 ± 1.111	7.443 ± 0.412	0.2920	116, 1171
EW([N II]) (Å)	3.821 ± 0.378	3.477 ± 0.121	0.4446	115, 1170
EW([O III]) (Å)	23.17 ± 3.073	19.55 ± 0.905	0.0481	112, 1155
$D_n(4000)$	1.243 ± 0.022	1.253 ± 0.007	$<10^{-4}$	69, 753
$\log_{10}(\text{mass}/M_\odot)$	8.279 ± 0.060	8.273 ± 0.019	0.3589	118, 1185
SFR(Hα) ($M_\odot$ yr^{-1})	0.054 ± 0.006	0.098 ± 0.005	0.1725	109, 1066
S-SFR(Hα) (yr^{-1})	$(29.19 \pm 4.527) \times 10^{-11}$	$(46.37 \pm 2.713) \times 10^{-11}$	0.0269	109, 1066

NOTE.—Means, errors on the means, and KS test probabilities that the void and wall galaxies are drawn from the same parent population for the spectroscopic properties of void and wall galaxies in the nearby sample ($r < 72\ h^{-1}$ Mpc). The number of galaxies (void and wall) in each sample and subsample are listed next to the magnitude range heading as [N_V(void), N_W(wall)]. The KS test shows that void galaxies appear to have stronger emission line EWs than wall galaxies in all cases. The average difference between the means of the EWs and $D_n(4000)$s is about 2 σ_μ. However, the SFRs and stellar masses are not significantly different. Only the bright void galaxy subsample shows a larger S-SFR(Hα) than wall galaxies.

[a] Small values of P correspond to a low probability that the two samples are drawn from the same parent population.

Tables 1 and 2 summarize the results of these tests for the distant and nearby samples, respectively. We present results for the whole sample, as well as for the samples split by absolute magnitude. These results are considered in detail below.

3.1. *Equivalent Widths*

In Tables 1 and 2, statistics of the EWs of the different lines (Hα, [O II] [where possible], Hβ, [N II], and [O III]) and samples (distant, nearby, bright, and faint) are given. In Figures 1 and 2, we show normalized histograms of EW(Hα) and EW([O II]) for the different samples. The solid lines correspond to the void galaxies and the dotted lines to the wall galaxies.

Void galaxies have average values of EW(Hα) of 19.14 ± 0.68 in the distant sample, whereas wall galaxies have average values of EW(Hα) $= 11.77 \pm 0.16$. The quoted errors are the errors on the means, and these will be quoted throughout. In the nearby sample, the values are higher, EW(Hα) $= 35.31 \pm 0.26$ (void) and 26.18 ± 0.65 (wall). The values for EW([O II]) in the distant sample are 14.26 ± 0.40 (void) and 9.44 ± 0.09 (wall). In all the distant samples, we find that void galaxies have, on average, larger EWs than wall galaxies with differences in the means >5 σ_μ. In the nearby samples, the statistical significance of this difference is somewhat lower, roughly 2 σ_μ, because of the smaller sample size.

The statistical significance of the EW(Hα) differences between void and wall galaxies is also quantified through a KS test. For the distant samples, it is very unlikely that the void and wall galaxies are drawn from the same parent population ($P < 10^{-4}$). In the case of the nearby samples, only the faint subsample shows a large probability ($P = 0.37$) of being drawn from the same parent population. We attribute this in part to the decrease in the number of galaxies in this sample.

As in Rojas et al. (2004), we also test that the star formation properties of void versus wall galaxies are not simply explained by a shift in the morphological mix of galaxies. Galaxies with Sérsic index $n < 1.8$ have surface brightness profiles that resemble spirals, while galaxies with Sérsic index $n > 1.8$ are more like ellipticals. When we split the void and wall galaxy samples by Sérsic index at $n = 1.8$ and again compare their EWs, void galaxies persist in having statistically significant, larger EWs.

3.2. $D_n(4000)$

From Tables 1 and 2, we see that there is a very low probability ($P < 10^{-4}$) that the distributions of $D_n(4000)$ of void and

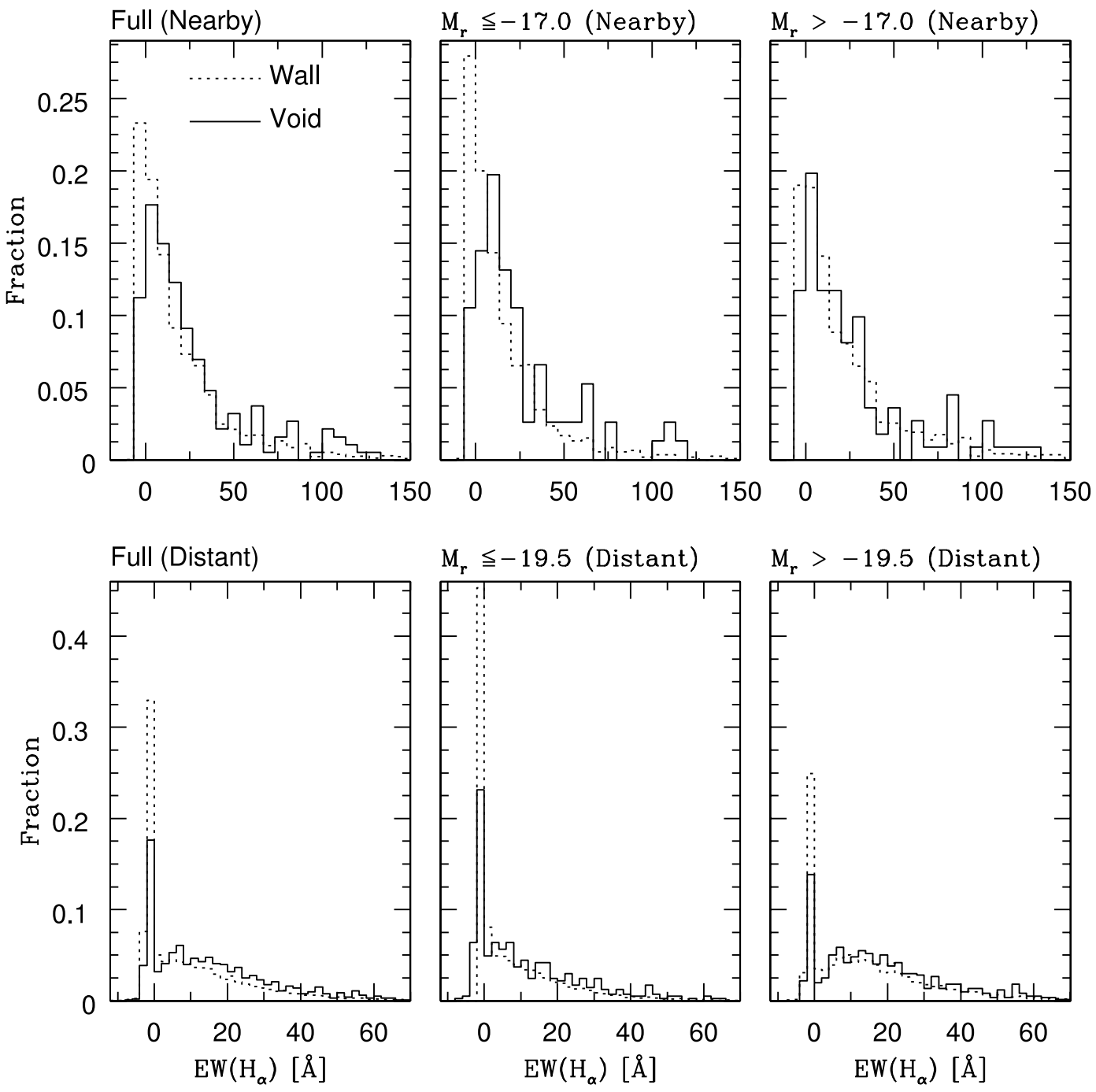

FIG. 1.—Distribution of Hα EWs showing the normalized fraction of void (*solid lines*) and wall galaxies (*dotted lines*) as a function of EW(Hα). *Top row*: results for the nearby ($r < 72\ h^{-1}$ Mpc) galaxies; *bottom row*: results for the distant ($100 \leq r \leq 260\ h^{-1}$ Mpc) galaxies. First, second, and third columns are the full, bright, and faint samples, respectively. The fraction of galaxies per 6.5 Å (*nearby*) and 2 Å (*distant*) bin of EW(Hα) is shown on the *y*-axis. The KS statistic reveals that the distant void galaxy (bright, faint, and full) and respective wall galaxy samples are very different from one another, with a probability of <0.01% that they are drawn from the same parent population. In the case of the nearby galaxies, only the faint galaxy distributions (*top right panel*) have a higher probability ($P \lesssim 0.37$) of being similar. [*See the electronic edition of the Journal for a color version of this figure.*]

wall galaxies (distant and nearby) are drawn from the same parent population.

In Figure 3 we show the distributions of $D_n(4000)$ for the void and wall galaxy samples. We observe two noticeable features: (1) all samples of void galaxies have on average smaller $D_n(4000)$ than wall galaxies, and (2) there is an obvious deficit of early-type galaxies in the nearby samples, which is observed in the amplitude of the distributions for $D_n(4000) \gtrsim 1.5$. This is consistent with the results of Rojas et al. (2004), where we found few galaxies with Sérsic and concentration indices typical of early-type galaxies. The lower values of $D_n(4000)$ indicate that there is more recent star formation in the void galaxies.

4. DERIVED SPECTROSCOPIC PROPERTIES

An alternative way of comparing the spectral properties of void and wall galaxies is to convert the spectral lines into estimated SFRs. This is discussed below in § 4.2. Because void galaxies are typically of lower luminosity and stellar mass, it is

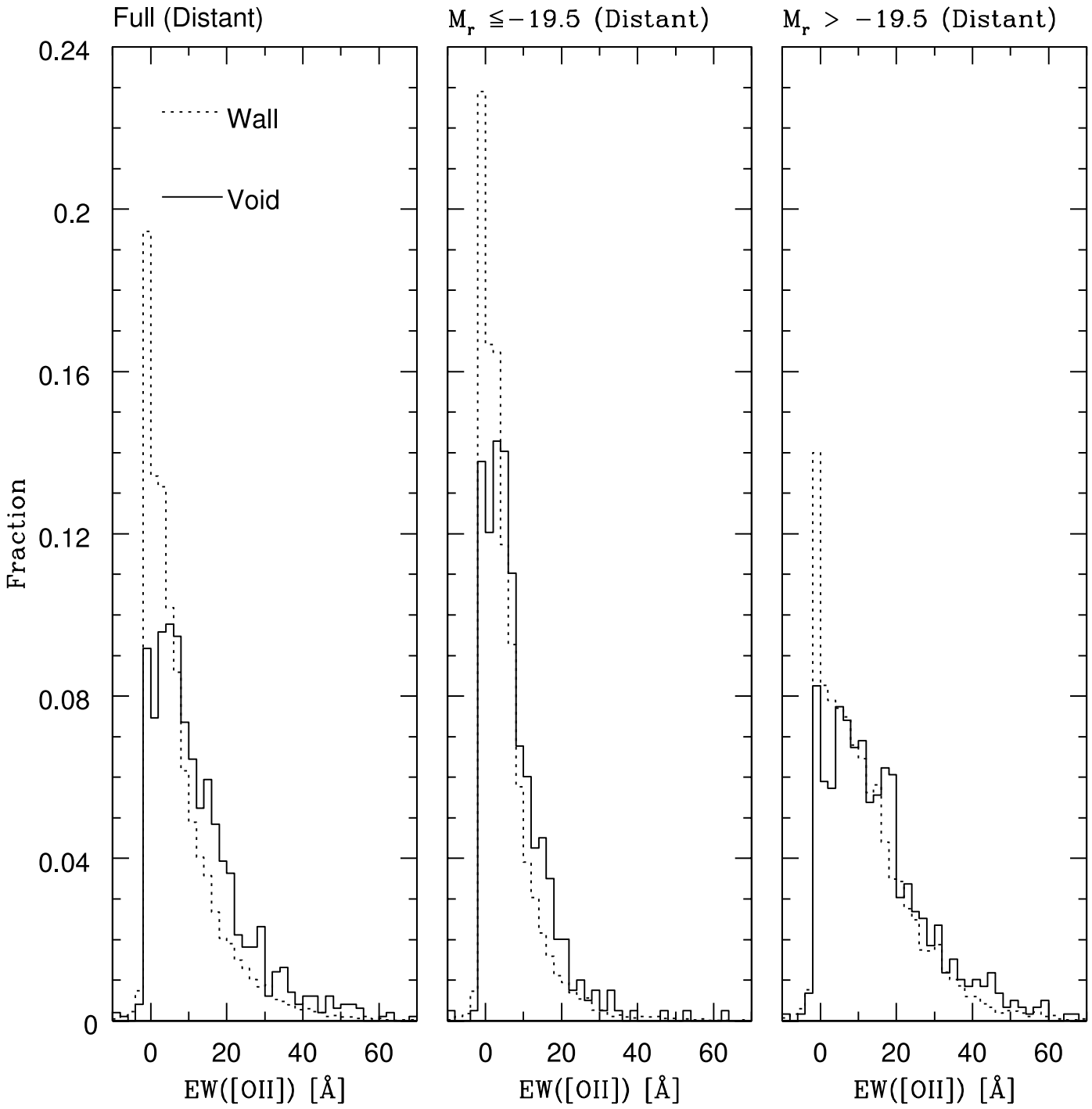

FIG. 2.—Distribution of [O II] EWs showing the normalized fraction of void (*solid lines*) and wall galaxies (*dotted lines*) as a function of EW([O II]). First, second, and third figures are the full, bright, and faint distant samples, respectively. The fraction of galaxies per 2 Å bin of EW([O II]) is shown on the *y*-axis. The KS statistic reveals that the distant void galaxy (bright, faint, and full) and respective wall galaxy samples are very different from one another, with a probability of <0.01% that they are drawn from the same parent population. [*See the electronic edition of the Journal for a color version of this figure*.]

important to normalize the SFR; thus, we also compute the "specific" SFR (S-SFR), i.e., the SFR divided by the mass of the galaxy. For the S-SFRs, we obviously require masses, and we discuss this first.

4.1. *Stellar Masses*

The integrated stellar masses for 70% of our sample come from K03's library of stellar masses. They estimate the stellar masses by taking the product of the model predicted *z*-band stellar mass-to-light ratio $(M/L)_z$ and the respective dust-corrected luminosity of the galaxy. The model used by K03 to predict the $(M/L)_z$ and stellar masses is based on median likelihood estimates from their library of Monte Carlo realizations of different star formation histories. Thirty percent of the galaxies are missing from K03, as they analyzed galaxies from DR1 (Abazajian et al. 2003), while our sample is from a larger database (Blanton et al. 2003b; sample10). For the additional 30% of galaxies, we use the use the *z*-band absolute magnitude to estimate the

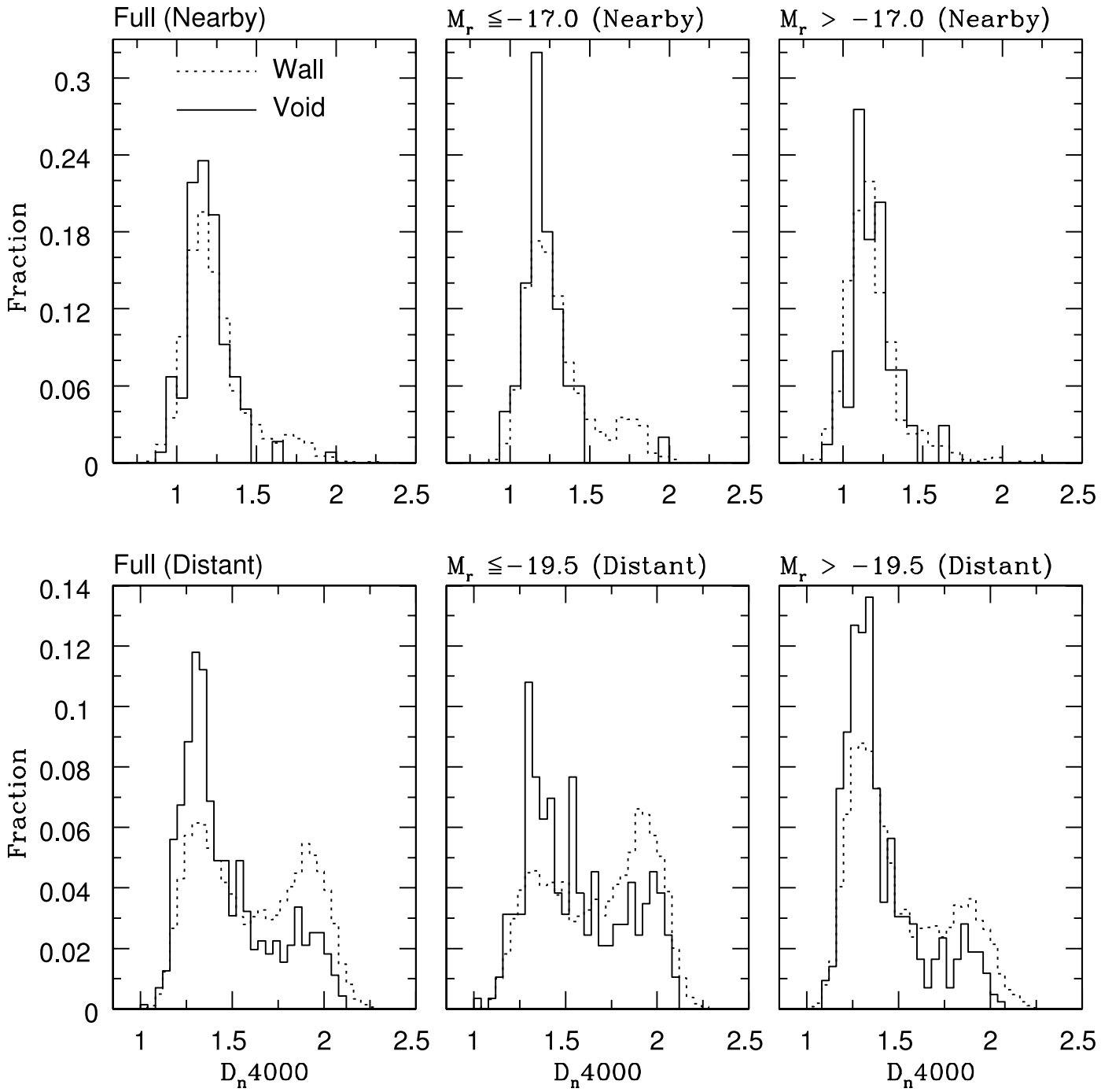

FIG. 3.—Distribution of the 4000 Å Balmer break showing the normalized fraction of void (*solid lines*) and wall galaxies (*dotted lines*) as a function of $D_n(4000)$. *Top row*: results for the nearby ($r < 72\ h^{-1}$ Mpc) galaxies; *bottom row*: results for the distant ($100 \leq r \leq 260\ h^{-1}$ Mpc) galaxies. First, second, and third columns are the full, bright, and faint samples, respectively. The fraction of galaxies per 0.067 (*nearby*) and 0.04 (*distant*) bin of $D_n(4000)$ is shown on the *y*-axis. The KS statistic reveals that the distant and nearby void galaxy (bright, faint, and full) and respective wall galaxy samples are very different from one another, with a probability of <0.01% that they are drawn from the same parent population. [*See the electronic edition of the Journal for a color version of this figure*.]

mass, using the nearly linear relationship between this magnitude and the logarithm of the estimated stellar mass (K03). This relationship is shown in Figure 4. The scatter is restricted to a narrow range about the line of best fit [$\log_{10}(\mathrm{mass}/M_\odot) = -0.5134M_z - 0.01581$]. Using this fit, we estimate that we can measure typical stellar masses to within a factor of 5.

In Figure 5 we show the normalized histograms of the masses for all the samples. The differences between these distributions are listed in Tables 1 and 2. It can be readily seen in the distant sample that, on average, void galaxies have smaller stellar masses than wall galaxies [$\log(M/M_\odot) = 10.13 \pm 0.02$ as opposed to $\log(M/M_\odot) = 10.43$]. The KS test shows that it is very unlikely that void galaxies are drawn from the same parent population ($P < 10^{-4}$). However, in the nearby samples the mean values of the void and wall galaxy masses are more similar [$\log(M/M_\odot) = 8.69 \pm 0.06$ vs. $\log(M/M_\odot) = 8.80 \pm 0.02$].

4.2. *Star Formation Rates*

To estimate SFRs, the basic steps are to (1) measure the flux in each line, (2) convert the flux into a luminosity, and (3) apply

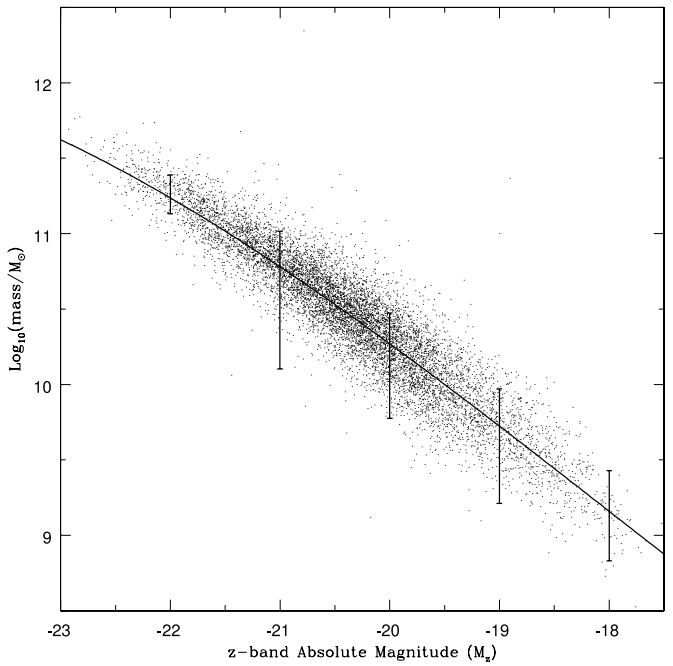

FIG. 4.—Plot of $\log_{10}(\text{mass}/M_{\odot})$ vs. z-band absolute magnitude using Kauffmann et al. (2003) stellar masses (*points*). Error bars are the 1 σ errors of stellar masses in bins $\Delta M_z = 1$ wide. The solid line is a least-squares fit. We use this linear fit to estimate the stellar masses of other galaxies in our sample using their z-band flux. [*See the electronic edition of the Journal for a color version of this figure*.]

Kennicutt's (1998) formulas for SFRs. We employ the SDSS SFR prescription of Hopkins et al. (2003) with minor variations, as discussed below. We calculate the SFR from the line flux of both Hα and [O II] when both are observed.

The flux is obtained via

$$F = \sqrt{2\pi}\sigma\kappa \times 10^{-17} \text{ ergs cm}^{-2} \text{ s}^{-1}, \quad (1)$$

where σ and κ are the widths and heights of the Gaussian fit to the respective line. These parameters are measured by the SDSS spectroscopic data analysis pipeline. The fit κ is in units of ergs cm^{-2} s^{-1} Å and σ in units of angstroms.

The next step is to compute the respective luminosity (L) using

$$L = 4\pi D_L^2 F \text{ ergs s}^{-1}, \quad (2)$$

where D_L is the luminosity distance in units of centimeters.

Finally, using Kennicutt's (1998) formula for the Hα flux valid in the case B recombination (Osterbrock 1989) with a Salpeter (1955) initial mass function, we compute the SFR using

$$\text{SFR} = 7.9 \times 10^{-42} L \, M_{\odot} \text{ yr}^{-1}, \quad (3)$$

and for [O II] we use Kennicutt's (1998) calibration

$$\text{SFR} = 1.4 \times 10^{-41} L \, M_{\odot} \text{ yr}^{-1}. \quad (4)$$

There are several important corrections that must be accounted for. These include stellar absorption corrections, aperture effects, dust, and smearing. We discuss each of these below.

We begin by correcting the emission line EWs for absorption lines in the stellar continua. In principle, one could use a factor (EW$_c$) appropriate for the type of galaxy being studied, if the latter were known. Miller & Owen (2002) found that this correction varies from 0.9 Å (E type) to 4.1 Å (extreme spirals). Similar to Hopkins et al. (2003), we apply an "average" correction to the observed Balmer line EW that is approximately correct for the whole sample, but which is not precisely correct for any individual galaxy. Some of the apparently negative SFRs obtained for our sample can be attributed to this uncertainty. Hopkins et al. (2003) adopt a value of EW$_c = 1.3$ Å for their analysis of the SDSS DR1 sample. In our case, a correction of EW$_c = 1.4$ Å is more appropriate for the morphological mix of our galaxies (C. Tremonti 2004, private communication). This correction is then converted to a flux correction via $F_c = [(\text{EW} + \text{EW}_c)/\text{EW}]F$, where F is the observed line flux (eq. [1]), and F_c is the corrected line flux.

The next step is to correct the stellar absorption corrected flux F_c for aperture effects. Because emission detected through the 3″ spectroscopic fiber depends on the redshift of the galaxy (nearby a smaller area of the galaxy is detected, and at greater distances a larger area can be detected), we need to scale the spectroscopic line flux to correspond to a consistent aperture (assuming that the spectrum of the galaxy does not spatially vary). This is accomplished by scaling F_c by $10^{0.4[M_{r(\text{spec})} - M_{r(\text{Pet})}]}$, where $M_{r(\text{spec})}$ and $M_{r(\text{Pet})}$ are the synthetic and Petrosian[3] k-corrected SDSS r-band absolute magnitudes, respectively. Therefore, the stellar absorption and aperture corrected flux (F_c') is

$$F_c' = F_c \times 10^{0.4[M_{r(\text{spec})} - M_{r(\text{Pet})}]} \text{ ergs s}^{-1}. \quad (5)$$

Note that for $F_c'(\text{H}\beta)$, we use the g-band absolute magnitude when estimating the aperture corrections. For all other fluxes, the r band is used.

By far the largest correction (about a factor of 10) consists of accounting for obscuration by dust. Here we apply the Fitzpatrick (1999) parameterization and compute the color excess $E(B-V)$ from the Balmer decrement given by $\tau_{\text{Balmer}} = \ln[F_c'(\text{H}\alpha)/F_c'(\text{H}\beta)/2.87]$, where $F_c'(\text{H}\alpha)$ and $F_c'(\text{H}\beta)$ are the stellar absorption and aperture corrected Hα and Hβ fluxes, respectively, and

$$E(B-V) = 1.086\tau_{\text{Balmer}}/1.17. \quad (6)$$

Significant underestimates of the derived SFRs would be expected, if this effect were unaccounted for. In the case of SFRs derived from the [O II] line, the situation is even more severe because of the larger variation of τ_{Balmer} (Gallagher et al. 1989; Kennicutt 1992). This implies that SFRs of dustier galaxies will have considerably larger corrections (increase in flux) than dust-poor galaxies. We find that void galaxies are relatively dust poor, and therefore wall galaxies have the largest increase in flux due to reddening corrections. These corrections are quite significant: wall galaxies have an average factor of 13 increase in flux over void galaxies, which have a factor of 9 increase, after all the relevant corrections are applied.

Given an estimate of the color excess for each galaxy, we can deredden the Hα, Hβ, and [O II] fluxes using the R-dependent Galactic extinction curve of Fitzpatrick & Massa (1999) with a

[3] The magnitudes that are measured from the SDSS are Petrosian magnitudes (Petrosian 1976). The Petrosian magnitude is the total amount of flux within a circular aperture whose radius depends on the shape of the galaxy light profile, i.e., the size of the aperture is not fixed so galaxies of the same type are observed out to the same physical distance at all redshifts. More details are given in Stoughton et al. (2002).

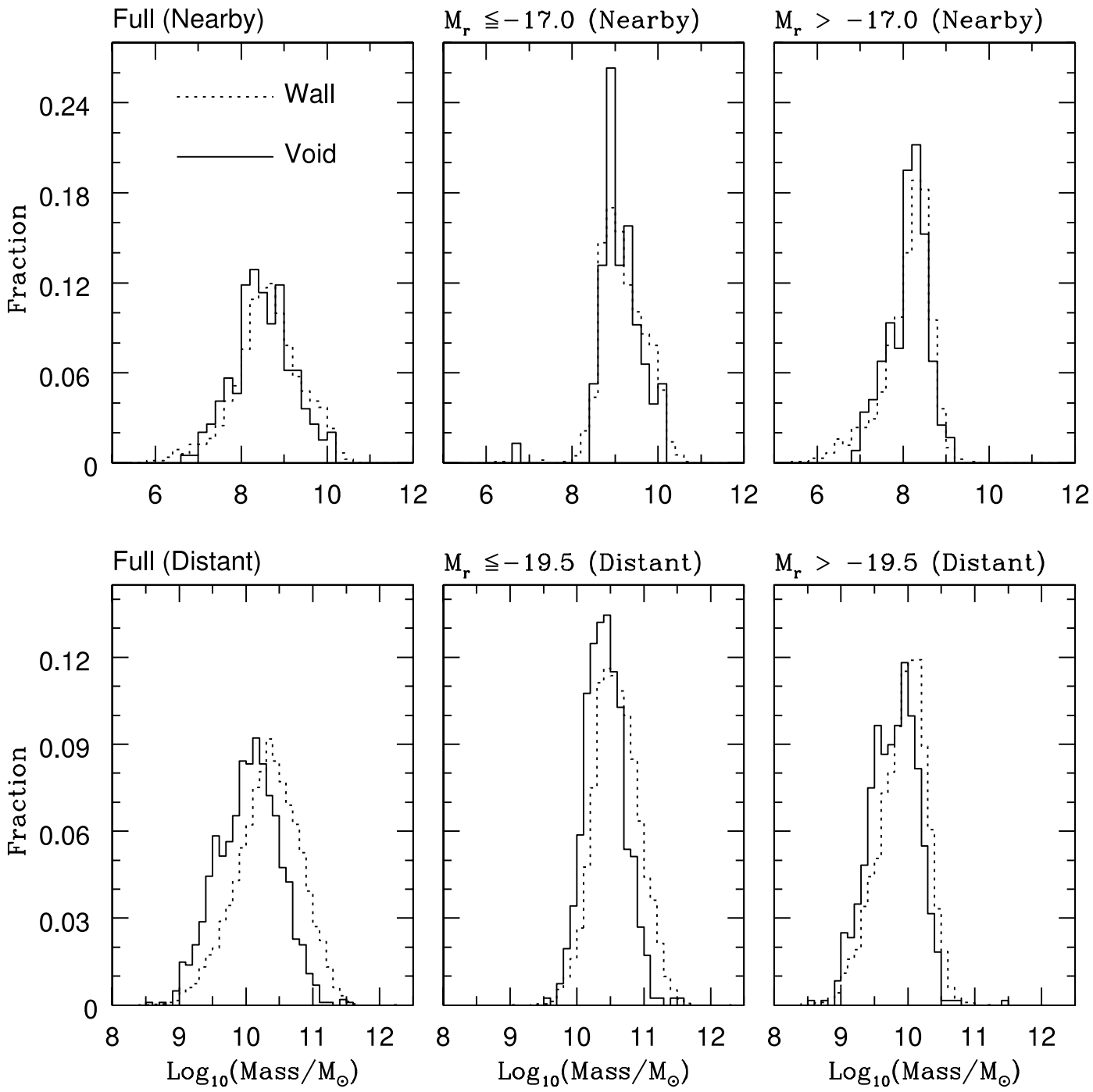

FIG. 5.—Stellar Mass Distribution showing the normalized fraction of void (*solid lines*) and wall galaxies (*dotted lines*) as a function of $\log_{10}(\mathrm{mass}/M_\odot)$. *Top row*: results for the nearby ($r < 72\ h^{-1}$ Mpc) galaxies; *bottom row*: results for the distant ($100 \leq r \leq 260\ h^{-1}$ Mpc) galaxies. First, second, and third columns are the full, bright, and faint samples, respectively. The fraction of galaxies per 5 $M_\odot$ (*nearby*) and 10 $M_\odot$ (*distant*) bin of $\log_{10}(\mathrm{mass}/M_\odot)$ is shown on the *y*-axis. The KS statistic reveals that the distant void galaxy (bright, faint, and full) and respective wall galaxy samples are very different from one another, with a probability of $<0.01\%$ that they are drawn from the same parent population. In the case of the nearby galaxies, only the bright galaxy distributions have a higher probability ($P \lesssim 0.36$) of being similar. [*See the electronic edition of the Journal for a color version of this figure*.]

value of $R = 3.1$. The dust-corrected F_c' is now substituted into equation (2), to compute the respective absorption, aperture, and dust-corrected luminosities from which the SFRs are derived using equation (3).

Our analysis also accounts for smearing in the SDSS spectroscopic observing procedure (Stoughton et al. 2002). It consists of four-minute spectroscopic observations performed while the telescope dithers for the purpose of correcting for light losses from the 3″ fiber aperture. For galaxies, about 1/3 of their light is contained within the 3″ fiber aperture. Although the systematic differences between smear-corrected and original spectra are only about 10% (Hopkins et al. 2003), the increase in the reported flux is generally about a factor of 2. Fortunately, this was accounted for by using the *r*-band Petrosian magnitude in the aperture-correction factor (this essentially scales the spectrum to match the photometry, which is more reliable). An inherent assumption is that the EW(Hα) and reddening are constant across the Petrosian aperture.

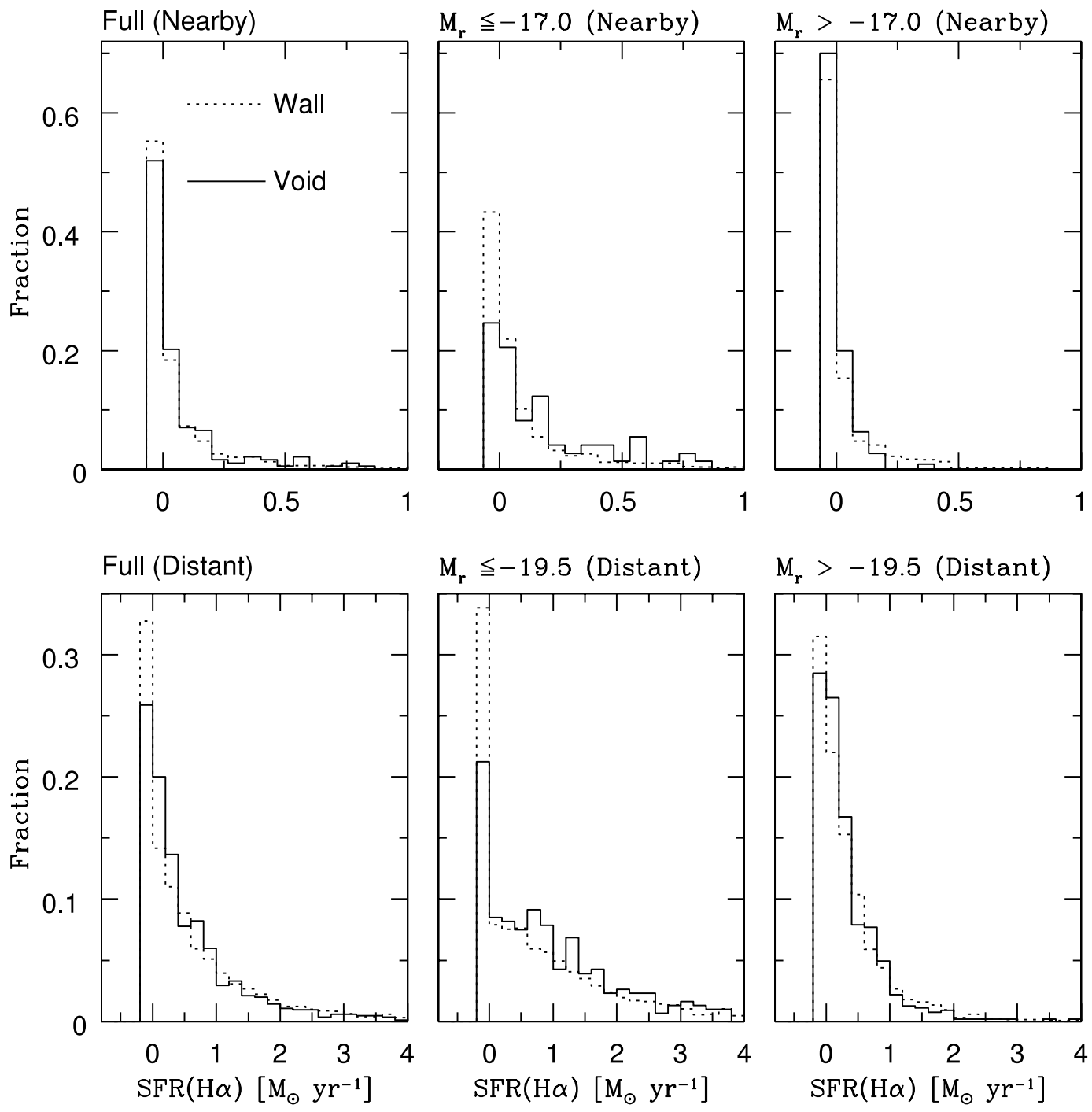

FIG. 6.—Distribution of Hα SFRs showing the normalized fraction of void (*solid lines*) and wall galaxies (*dotted lines*) as a function of SFR(Hα). *Top row*: results for the nearby ($r < 72\ h^{-1}$ Mpc) galaxies; *bottom row*: results for the distant ($100 \leq r \leq 260\ h^{-1}$ Mpc) galaxies. First, second, and third columns are the full, bright, and faint samples, respectively. The fraction of galaxies per 0.067 $M_\odot$ yr^{-1} bin of SFR(Hα) is shown on the *y*-axis. The KS statistic reveals that the distant void galaxy (bright and full) and respective wall galaxy samples are very different from one another, with a probability of <0.01% that they are drawn from the same parent population. [*See the electronic edition of the Journal for a color version of this figure.*]

In Tables 1 and 2, we summarize the results from the SFR estimates and compare the SFR normalized distributions for void and wall galaxies in Figure 6 [SFR(Hα)] and Figure 7 [SFR([O II])]. As noted above, SFR([O II]) can only be determined from the distant sample, as [O II] does not appear in the spectra of most of the nearby sample of galaxies.

In the distant sample, the wall galaxies have slightly higher SFR than the void galaxies ($0.747 \pm 0.007\ M_\odot\ \mathrm{yr}^{-1}$ vs. $0.734 \pm 0.025\ M_\odot\ \mathrm{yr}^{-1}$ for Hα, and $0.488 \pm 0.006\ M_\odot\ \mathrm{yr}^{-1}$ vs. $0.448 \pm 0.015\ M_\odot\ \mathrm{yr}^{-1}$ for [O II]). However, in the nearby sample, the void galaxies have slightly higher SFR than the wall galaxies. Note that comparing SFRs is a bit misleading, because the void galaxies are typically fainter than the wall galaxies and have smaller masses (§ 4.1), and thus would not be expected to have SFRs that are as high. A fairer comparison is to use the specific SFR, which we discuss below.

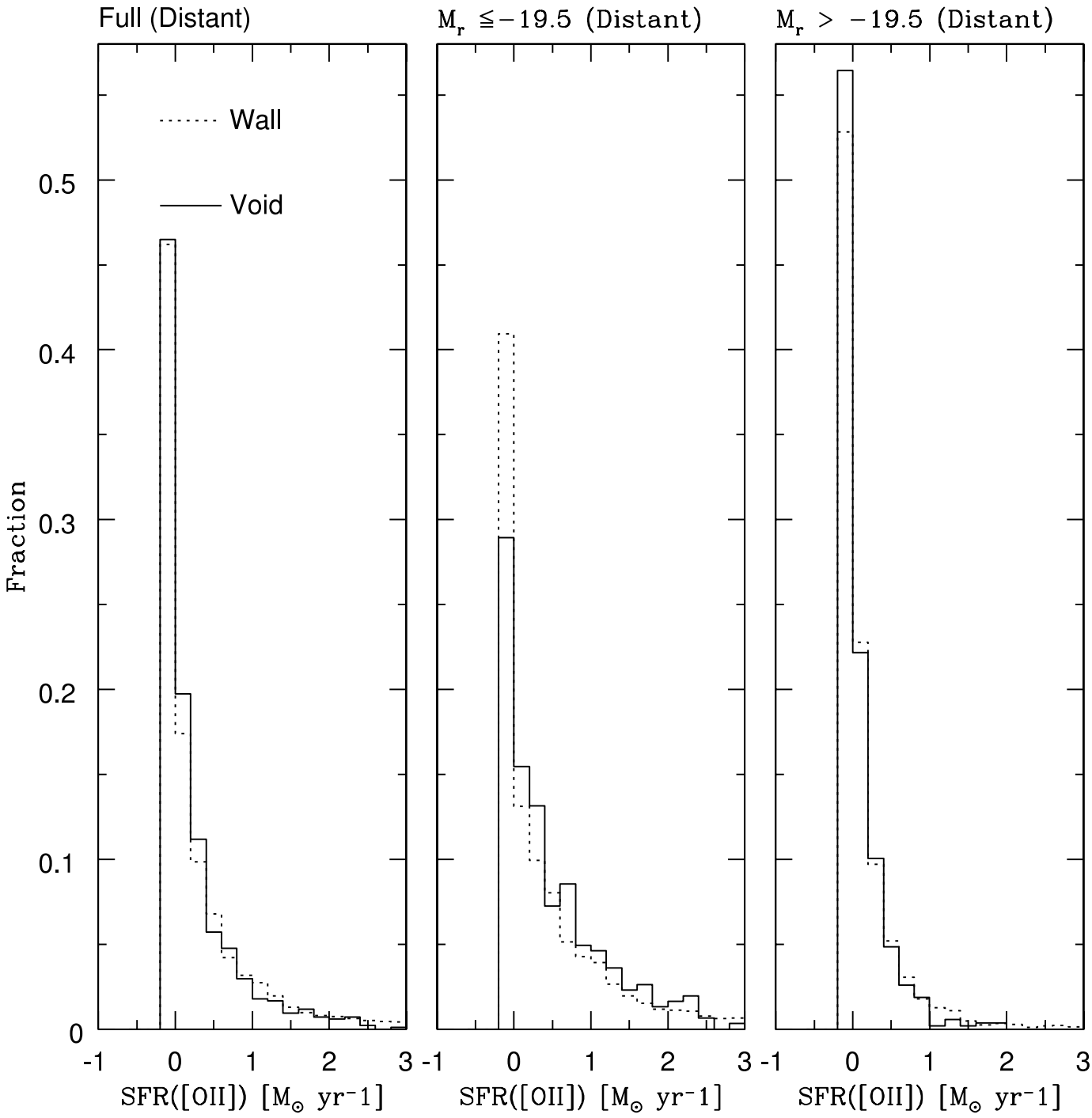

FIG. 7.—Distribution of [O II] SFRs showing the normalized fraction of void (*solid lines*) and wall galaxies (*dotted lines*) as a function of SFR([O II]). First, second, and third figures are the full, bright, and faint distant samples, respectively. The fraction of galaxies per 0.067 $M_\odot$ yr^{-1} bin of SFR([O II]) is shown on the *y*-axis. The KS statistic reveals that the distant void galaxy (bright and full) and respective wall galaxy samples are very different from one another, with a probability of <0.01% that they are drawn from the same parent population. [*See the electronic edition of the Journal for a color version of this figure*.]

Note that when computing the means, errors on the means, and the KS statistic, we include the negative SFRs in all the calculations. Negative SFRs are obtained either when emission lines are seen as absorption lines, or when the strength of the line is too weak and therefore dominated by noise. As discussed above, the use of an average stellar line correction probably causes some of these negative SFRs, because some galaxies will have their EWs overcorrected for Balmer absorption.

The only SFRs that are not included are those for which an estimate of the color excess was not possible because $F'_c(\mathrm{H}\alpha)/F'_c(\mathrm{H}\beta) < 0$. Our samples of void and wall galaxies are reduced by about 12% by this restriction.

4.3. *Specific Star Formation Rates*

The SFR per unit stellar mass (S-SFR) is perhaps a more informative spectral indicator for our purposes, because void galaxies are on average less luminous and have smaller stellar

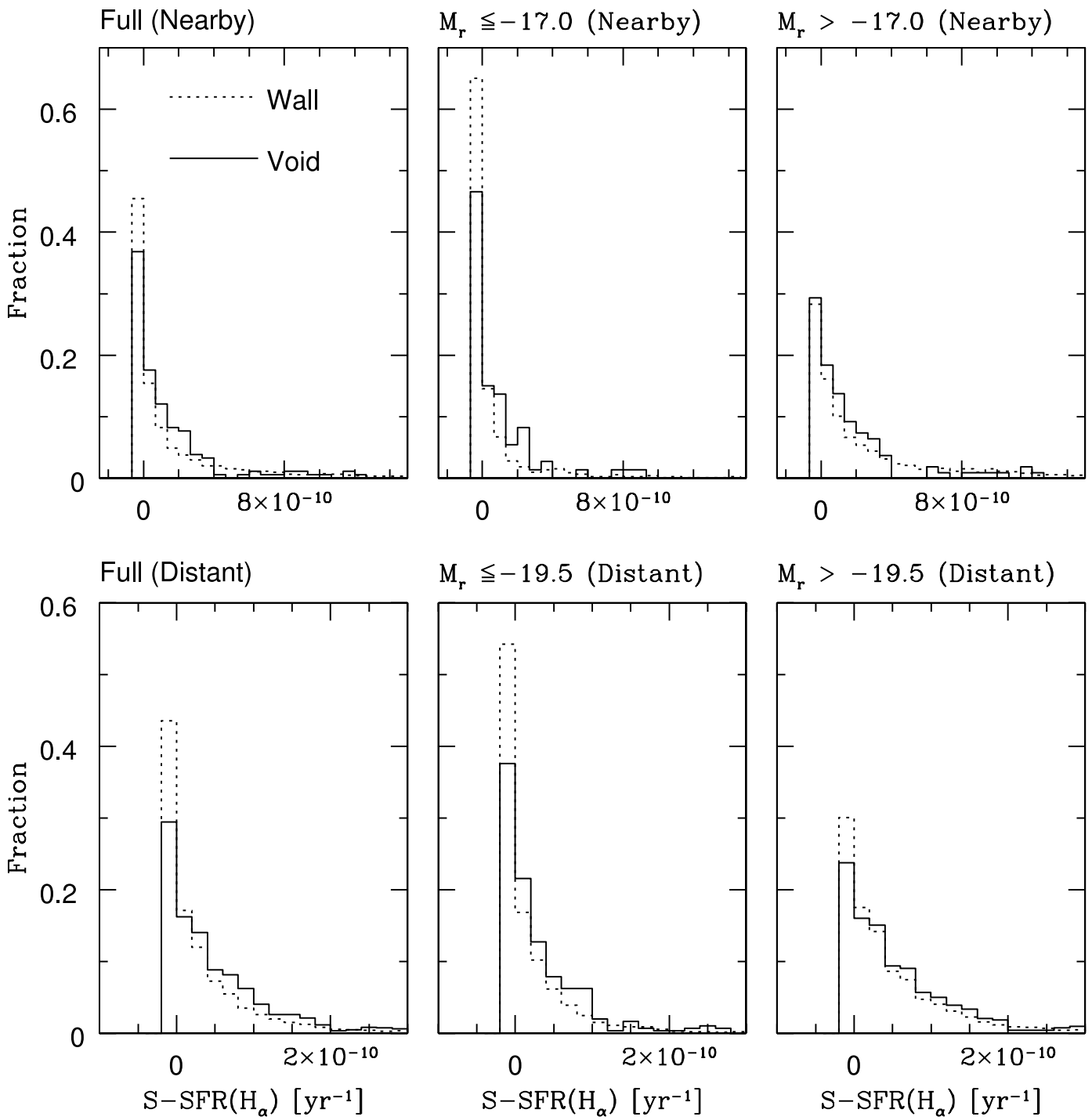

FIG. 8.—Distribution Hα S-SFRs showing the normalized fraction of void (*solid lines*) and wall galaxies (*dotted lines*) as a function of S-SFR(Hα). *Top row*: results for the nearby ($r < 72\ h^{-1}$ Mpc) galaxies; *bottom row*: results for the distant ($100 \leq r \leq 260\ h^{-1}$ Mpc) galaxies. First, second, and third columns are the full, bright, and faint samples, respectively. The fraction of galaxies per 10^{-10} yr^{-1} bin of S-SFR(Hα) is shown on the *y*-axis. The KS statistic reveals that the distant void galaxy (bright, faint, and full) and respective wall galaxy samples are very different from one another, with a probability of <0.01% that they are drawn from the same parent population. In the case of the nearby galaxies, only the bright galaxy distributions have a higher probability ($P \lesssim 0.027$) of being similar. [*See the electronic edition of the Journal for a color version of this figure.*]

masses. We estimate the S-SFRs using the stellar masses and the absorption, aperture, and dust-corrected SFRs as discussed above. Note again the caveats that the dust correction is a large effect, and that the fluxes are not individually corrected for Balmer absorption. Consistent with our analysis of the SFRs, we include negative S-SFRs in the calculation of the mean. Neither the negative SFRs nor the negative S-SFRs have a physical meaning, yet removal of the 11% of galaxies that have S-SFRs <0 would artificially shift the S-SFR distributions.

In Figures 8 and 9, we show the S-SFR distributions for the Hα and [O II] lines, respectively. In the distant samples (full, bright, and faint), including subsamples split by the Sérsic index, void galaxies have larger average S-SFRs(Hα) and S-SFRs([O II]) than wall galaxies. The KS test shows that the

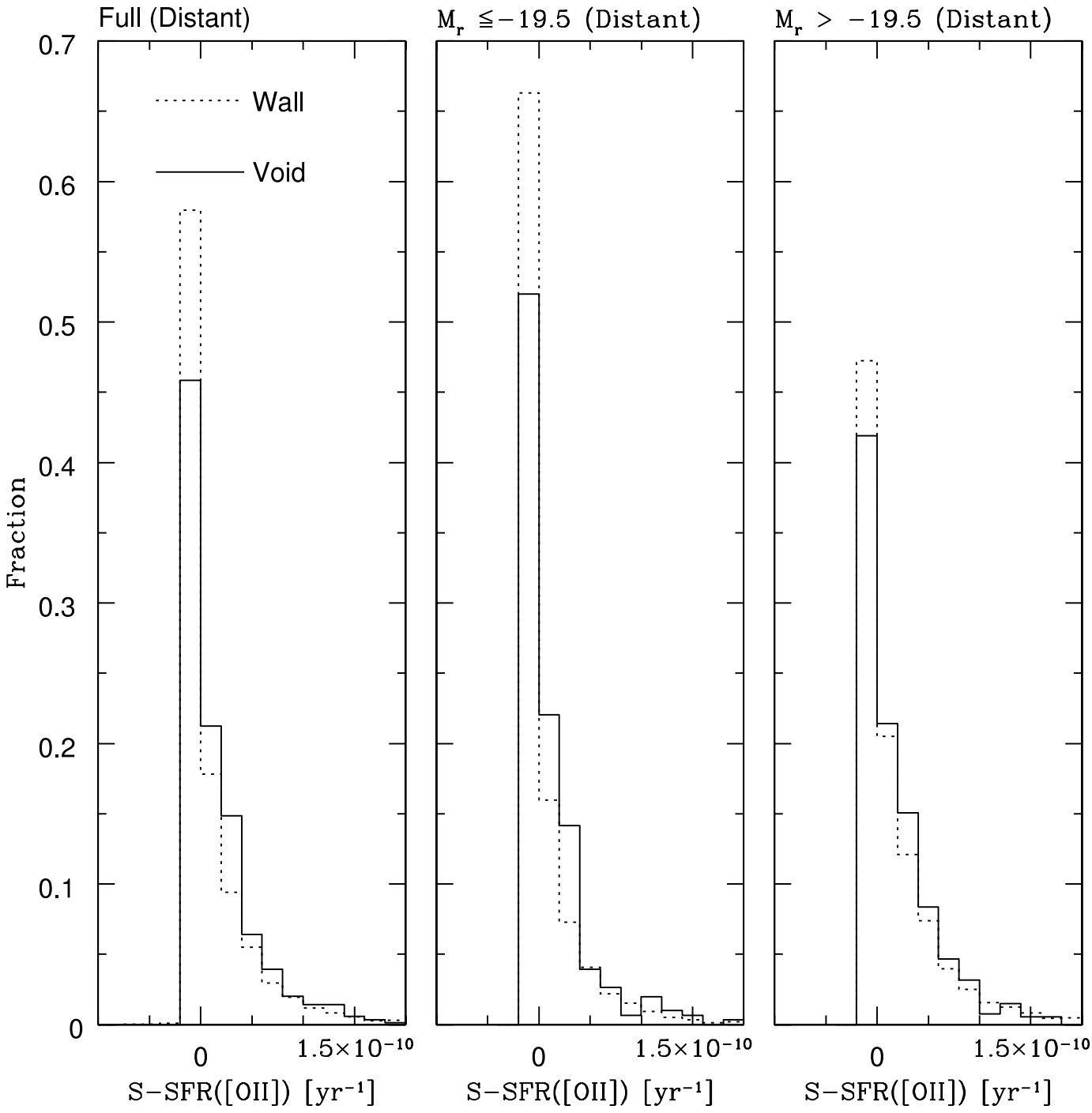

FIG. 9.—Distribution of [O II] S-SFRs showing the normalized fraction of void (*solid lines*) and wall galaxies (*dotted lines*) as a function of S-SFR([O II]). First, second, and third columns are the full, bright, and faint distant samples, respectively. The fraction of galaxies per 10^{-10} yr^{-1} bin of SFR([O II]) is shown on the *y*-axis. The KS statistic reveals that the distant void galaxy (bright, faint, and full) and respective wall galaxy samples are very different from one another, with a probability of $<0.034\%$ that they are drawn from the same parent population. [*See the electronic edition of the Journal for a color version of this figure*.]

probability of void and wall galaxies being derived from the same parent population is $<10^{-4}$. Thus, consistent with the results from the EWs, void galaxies are forming more stars per unit mass than the wall galaxies.

An apparent exception is that wall galaxies in the faint nearby sample have somewhat higher SFRs and S-SFRs than the void galaxies. However, comparison of the EWs yields the opposite result; void galaxies have stronger EWs, although the differences are within 1–2 σ. The photometric properties of these galaxies are also least distinct; the void galaxies are slightly bluer, but the morphological properties are very similar (Rojas et al. 2004). It is quite possible that the dust corrections applied to obtain the SFR are not applicable for this class of faint, $M_r < -17$, galaxies, or perhaps that the wall galaxies in this category are also somewhat isolated. A detailed study of the individual galaxies and/or a larger sample that can be more finely split as a function of density is required to study this category of galaxies in more detail.

5. DISCUSSION

We find that in all cases, distant or nearby, bright or faint, the void galaxies have higher EWs than galaxies that reside in higher density regions. In most cases, void galaxies also have higher S-SFRs than wall galaxies. EW measurements are less affected by the large uncertainties than the SFR and S-SFR calculations and, as such, are perhaps a more reliable indicator of the recent star formation histories of galaxies. In this section, we discuss these results and compare them with work from other groups.

The effect of a galaxy's environment on star formation has long been studied. Recent work has tended to focus on galaxies in environments that are more dense than the void galaxy sample that we present here. An exception is the work of Grogin & Geller (2000), who probed the SFR-density relation using a sample of 150 galaxies with values of $n/\bar{n} < 1$, i.e., $\delta\rho/\rho < 0.0$. Forty-six of these galaxies had $\delta\rho/\rho < -0.5$, which is close to meeting our definition of void galaxies. They found that the strength of EW(Hα) was 2–3 σ stronger than that of galaxies at higher environments, consistent with our results. We are able to probe to even lower density environments and find that the trend continues even more strongly.

Balogh et al. (2004) also studied the strength of EW(Hα) in a different range of environments, from groups to low-density regions. They consider both projected and three-dimensional density estimates, the latter on scales of 1.1 h^{-1} Mpc. They also find that the strength of EW(Hα) increases as density decreases. They find that rather than the whole population increasing in Hα, it is the fraction of galaxies that show measurable Hα that dominates this increase. Even so, in their most underdense environments, 30% of the galaxies still show very little emission, EW(Hα) < 4. We find that 12%–18% of the void galaxies have very little Hα emission. Their analysis of the variation of EW(Hα) with density on scales of 5.5 h^{-1} Mpc suggested that on these larger scales the difference between EW(Hα) in void and wall regions might be greater, consistent with our results.

Gómez et al. (2003) calculate SFRs and S-SFRs as a function of density. They use a projected density estimate rather than a density estimate in redshift space, so a direct comparison with our results is difficult, and they do not probe environments that are as underdense as those in this study. For example, their strongest Hα emitting galaxies have EW(Hα) of 19, which is the average value for our void sample. Nevertheless, they also find that SFR increases as the projected density decreases, although there is a large scatter. Lewis et al. (2002) perform a similar analysis using the 2dF Galaxy Redshift Survey and find very similar results. Gómez et al also examine whether the morphology density relation is the reason for this change in star formation. They find that late-type galaxies, as classified by the concentration index, have stronger SFR in lower density environments than in high-density environments, consistent with our findings and with results from Hashimoto et al. (1998), Couch et al. (2001), and Pimbblet et al. (2002). Kauffmann et al. (2004) also probe SFR as a function of density, although their lowest density bin includes more than 20% of their galaxy sample, whereas the void galaxy sample here includes only the lowest density 5%–8% of galaxies. These other authors see similar trends of SFR with density and high star formation in the lowest density regions, but in contrast to Balogh et al. (2004) and the results here, they claim that the trend in SFR only occurs on small, <2 h^{-1} Mpc, scales.

The observed photometric and spectroscopic properties of void galaxies generally agree with predictions from semianalytic models of structure formation (Benson et al. 2003) and scenarios in which galaxy–galaxy interactions govern galaxy evolution. These models attempt to include feedback effects from star formation. Void galaxies modeled in this fashion are bluer, more disklike, and have higher S-SFRs than objects in denser regions. Benson et al. (2003) find that the differences between void and wall galaxies in the simulations are due to the shift toward a smaller mass of the halo mass function in voids. Evidence for such a shift in the halo mass function is given by Goldberg et al. (2005), who estimate the halo mass function of our void galaxy sample and find that the best-fit theoretical mass function has mass underdensity $\delta = -0.6$, similar to the underdensity in galaxies.

How do these results fit into the galaxy formation scenario? One possibility is that void galaxies have formed recently and are young, hence the young stellar ages, low masses, and the active star formation. However, for galaxies to form in low-density environments at all, they would have to form before the matter in the voids flowed out to the higher density regions. The relative blueness and active star formation of the void galaxies would be explained if the void galaxies retained their gas supply over a longer period, allowing them to continue forming stars after their higher density counterparts have had their star formation shut down.

6. CONCLUSIONS

Using a sample of $\sim 10^3$ void galaxies identified from the SDSS with density contrast $\delta\rho/\rho < -0.6$, we are able to examine the environmental dependence of spectral properties of galaxies in extremely underdense regions.

We compare the equivalent widths of void and wall galaxies. Using this simple approach, we find that void galaxies have larger equivalent widths of Hα, [O II], Hβ, N II, and [O III]. This is the case regardless of distance to the galaxy, brightness, and morphological type. This would suggest that void galaxies have undergone recent star formation.

Void galaxies also show weaker Balmer decrements, as measured by $D_n(4000)$, which indicates that the stellar population includes a higher fraction of O and B stars. Thus, the emission line widths and continuum shape yield evidence of enhanced star formation over a range of timescales.

Specific star-formation rates (estimated SFRs normalized by the stellar mass of the galaxy) of void galaxies are generally higher than for wall galaxies. Unnormalized SFRs are similar or slightly higher for wall galaxies than void galaxies, but the void galaxies tend to have smaller stellar masses.

These spectroscopic results corroborate the photometric evidence given by Rojas et al. (2004) that void galaxies are bluer than wall galaxies of similar luminosity and morphology.

Thus, we show that the trend of increasing SFR with decreasing density, seen heretofore in denser regions, does indeed continue into the rarefied environment of voids.

Funding for the creation and distribution of the SDSS Archive has been provided by the Alfred P. Sloan Foundation, the Participating Institutions, the National Aeronautics and Space Administration, the National Science Foundation, the US Department of Energy, the Japanese Monbukagakusho, and the Max Planck Society.

The SDSS (http://www.sdss.org/) is managed by the Astrophysical Research Consortium (ARC) for the Participating Institutions. The Participating Institutions are The University of Chicago, Fermilab, the Institute for Advanced Study, the Japan Participation Group, The Johns Hopkins University, the Korean

Scientist Group, Los Alamos National Laboratory, the Max-Planck-Institute for Astronomy (MPIA), the Max-Planck-Institute for Astrophysics (MPA), New Mexico State University, University of Pittsburgh, Princeton University, the United States Naval Observatory, and the University of Washington.

We thank Christy Tremonti and Andrew Hopkins for useful conversations and for assistance with the systematics in the SFR calculations. We thank the anonymous referee for several helpful suggestions. M. S. V. acknowledges support from NSF grant AST-0071201 and a grant from the John Templeton Foundation.

REFERENCES

Abazajian, K., et al. 2003, AJ, 126, 2081
———. 2004, AJ, 128, 502
Balogh, M. L., Couch, W. J., Smail, I., Bower, R. G., & Glazebrook, K. 2002, MNRAS, 335, 10
Balogh, M. L., Morris, S. L., Yee, H. K. C., Carlberg, R. G., & Ellingson, E. 1997, ApJ, 488, L75
———. 1999, ApJ, 527, 54
Balogh, M. L., Schade, D., Morris, S. L., Yee, H. K. C., Carlberg, R. G., & Ellingson, E. 1998, ApJ, 504, L75
Balogh, M. L., et al. 2004, MNRAS, 348, 1355
Benson, A. J., Hoyle, F., Torres, F., & Vogeley, M. S. 2003, MNRAS, 340, 160
Blanton, M. R., Lin, H., Lupton, R. H., Maley, F. M., Young, N., Zehavi, I., & Loveday, J. 2003a, AJ, 125, 2276
Blanton, M. R., et al. 2003b, ApJ, 594, 186
———. 2003c, ApJ, 592, 819
Broadhurst, T. J., Ellis, R. S., & Glazebrook, K. 1992, Nature, 355, 55
Broadhurst, T. J., Ellis, R. S., & Shanks, T. 1988, MNRAS, 235, 827
Bruzual, G. 1983, ApJ, 273, 105
Colless, M., Ellis, R. S., Taylor, K., & Hook, R. N. 1990, MNRAS, 244, 408
Couch, W. J., Balogh, M. L., Bower, R. G., Smail, I., Glazebrook, K., & Taylor, M. 2001, ApJ, 549, 820
Couch, W. J., & Sharples, R. M. 1987, MNRAS, 229, 423
da Costa, L. N., et al. 1998, AJ, 116, 1
Dressler, A. 1980, ApJ, 236, 351
Dressler, A., Thompson, I. B., & Shectman, S. 1985, ApJ, 288, 481
Eisenstein, D. J., et al. 2001, AJ, 122, 2267
El-Ad, H., & Piran, T. 1997, ApJ, 491, 421
Falco, E. E., et al. 1999, PASP, 111, 438
Fitzpatrick, E. L. 1999, PASP, 111, 63
Fitzpatrick, E. L., & Massa, D. 1999, ApJ, 525, 1011
Fukugita, M., Ichikawa, T., Gunn, J. E., Doi, M., Shimasaku, K., & Schneider, D. P. 1996, AJ, 111, 1748
Gallagher, J. S., Hunter, D. A., & Bushouse, H. 1989, AJ, 97, 700
Goldberg, D. M., Jones, T. D., Hoyle, F., Rojas, R. R., Vogeley, M. S., & Blanton, M. R. 2005, ApJ, 621, 643
Gómez, P. L., et al. 2003, ApJ, 584, 210
Grogin, N. A., & Geller, M. J. 1999, AJ, 118, 2561
———. 2000, AJ, 119, 32
Gunn, J. E., et al. 1998, AJ, 116, 3040
Hashimoto, Y., & Oemler, A. J. 1999, ApJ, 510, 609
Hashimoto, Y., Oemler, A. J., Lin, H., & Tucker, D. L. 1998, ApJ, 499, 589
Hogg, D. W., Finkbeiner, D. P., Schlegel, D. J., & Gunn, J. E. 2001, AJ, 122, 2129
Hopkins, A. M., et al. 2003, ApJ, 599, 971
Hoyle, F., Rojas, R. R., Vogeley, M. S., & Brinkmann, J. 2005, ApJ, 620, 618
Hoyle, F., & Vogeley, M. S. 2002, ApJ, 566, 641
———. 2004, ApJ, 607, 751
Huchra, J. P. 1977, ApJ, 217, 928
Kauffmann, G., et al. 2003, MNRAS, 341, 33 (K03)
———. 2004, MNRAS, 353, 713
Kennicutt, R. C., Jr. 1992, ApJ, 388, 310
———. 1998, ARA&A, 36, 189
Kennicutt, R. C., & Kent, S. M. 1983, AJ, 88, 1094
Koo, D. C., & Kron, R. G. 1992, ARA&A, 30, 613
Lewis, I., et al. 2002, MNRAS, 334, 673
Miller, N. A., & Owen, F. N. 2002, AJ, 124, 2453
Osterbrock, D. E. 1989, The Astrophysics of Gaseous Nebulae and Active Galactic Nuclei (Mill Valley: Univ. Sci. Books)
Peterson, B. A., Ellis, R. S., Efstathiou, G., Shanks, T., Bean, A. J., Fong, R., & Zen-Long, Z. 1986, MNRAS, 221, 233
Petrosian, V. 1976, ApJ, 209, L1
Pier, J. R., Munn, J. A., Hindsley, R. B., Hennessy, G. S., Kent, S. M., Lupton, R. H., & Ivezić, Ž. 2003, AJ, 125, 1559
Pimbblet, K. A., Smail, I., Kodama, T., Couch, W. J., Edge, A. C., Zabludoff, A. I., & O'Hely, E. 2002, MNRAS, 331, 333
Poggianti, B. M., Smail, I., Dressler, A., Couch, W. J., Barger, A. J., Butcher, H., Ellis, R. S., & Oemler, A. J. 1999, ApJ, 518, 576
Postman, M., & Geller, M. J. 1984, ApJ, 281, 95
Rojas, R. R., Vogeley, M. S., Hoyle, F., & Brinkmann, J. 2004, ApJ, 617, 50
Salpeter, E. E. 1955, ApJ, 121, 161
Scranton, R., et al. 2002, ApJ, 579, 48
Smith, J. A., et al. 2002, AJ, 123, 2121
Solanes, J. M., Manrique, A., González-Casado, G., García-Gómez, C., Giovanelli, R., & Haynes, M. P. 2001, ApJ, 548, 97
Stoughton, C., et al. 2002, AJ, 123, 485
Strauss, M. A., et al. 2002, AJ, 124, 1810
SubbaRao, M., Frieman, J., Bernardi, M., Loveday, J., Nichol, B., Castander, F., & Meiksin, A. 2002, Proc. SPIE, 4847, 452
Tanaka, M., Goto, T., Okamura, S., Shimasaku, K., & Brinkmann, J. 2004, AJ, 128, 2677
Tran, K. H., Simard, L., Zabludoff, A. I., & Mulchaey, J. S. 2001, ApJ, 549, 172
Treu, T., Ellis, R. S., Kneib, J., Dressler, A., Smail, I., Czoske, O., Oemler, A., & Natarajan, P. 2003, ApJ, 591, 53
York, D. G., et al. 2000, AJ, 120, 1579
Zabludoff, A. I., & Mulchaey, J. S. 1998, ApJ, 496, 39